

# SCIENTIFIC REPORTS



OPEN

## A novel self-enhanced electrochemiluminescence immunosensor based on hollow Ru-SiO<sub>2</sub>@PEI nanoparticles for NSE analysis

Received: 09 December 2015

Accepted: 08 February 2016

Published: 26 February 2016

Limin Zhou<sup>1,2</sup>, Jianshe Huang<sup>1</sup>, Bin Yu<sup>1,3</sup> & Tianyan You<sup>1</sup>

Poly(ethylenimine) (PEI) and Ru(bpy)<sub>3</sub><sup>2+</sup>-doped silica (Ru-SiO<sub>2</sub>) nanoparticles were simply mixed together to prepare a novel self-enhanced electrochemiluminescence (ECL) composite of Ru-SiO<sub>2</sub>@PEI. The hollow Ru-SiO<sub>2</sub>@PEI nanoparticles were used to build an ECL immunosensor for the analysis of neuron specific enolase (NSE). PEI not only assembled on the surface of Ru-SiO<sub>2</sub> nanoparticles through the electrostatic interaction to act as co-reactant for Ru(bpy)<sub>3</sub><sup>2+</sup> ECL, but also provided alkaline condition to etch the Ru-SiO<sub>2</sub> nanoparticles to form the hollow Ru-SiO<sub>2</sub>@PEI nanoparticles with porous shell. The unique structure of the Ru-SiO<sub>2</sub>@PEI nanoparticles loaded both a large amount of Ru(bpy)<sub>3</sub><sup>2+</sup> and its co-reactant PEI at the same time, which shortened the electron-transfer distance, thereby greatly enhanced the luminous efficiency and amplified the ECL signal. The developed immunosensor showed a wide linear range from 1.0 × 10<sup>-11</sup> to 1.0 × 10<sup>-5</sup> mg mL<sup>-1</sup> with a low detection limit of 1.0 × 10<sup>-11</sup> mg mL<sup>-1</sup> for NSE. When the immunosensor was used for the determination of NSE in clinical human serum, the results were comparable with those obtained by using enzyme-linked immunosorbent assay (ELISA) method. The proposed method provides a promising alternative for NSE analysis in clinical samples.

Nowadays, cancer is one of the most threatening diseases for human beings<sup>1</sup>. Thus, the sensitive analysis of tumor biomarkers became greatly important since the level of biomarkers could provide useful information for early diagnosis and disease surveillance. Neuron specific enolase (NSE), a sensitive and reliable tumor marker for small cell lung cancer (SCLC)<sup>2</sup>, could be used to early diagnosis and assess the patient's recovery progress. Therefore, many methods have been proposed for the detection of NSE, including electrochemical immunoassay<sup>1,3-5</sup>, fluorescence immunoassay<sup>6,7</sup>, chemiluminescence immunoassay<sup>8,9</sup> etc<sup>10-14</sup>. However, developing new sensitive and simple method for the analysis of NSE is still important and meaningful.

As a powerful analytical method, electrochemiluminescence (ECL) has been widely used in environmental monitoring<sup>15,16</sup>, food safety<sup>17</sup>, bioanalysis<sup>18-25</sup>, and so forth<sup>26,27</sup> due to its high sensitivity, simple set-up and absence of background optical signal. Among the ECL luminophores, Ru(bpy)<sub>3</sub><sup>2+</sup> and its derivatives are the most extensively studied luminophores for their high ECL efficiency and good stability in aqueous solution. Ru(bpy)<sub>3</sub><sup>2+</sup>-doped silica (Ru-SiO<sub>2</sub>) nanoparticles have attracted much attention due to that each Ru-SiO<sub>2</sub> nanoparticle contained a large amount of Ru(bpy)<sub>3</sub><sup>2+</sup> molecules, which could greatly enhance the ECL signal. The Ru-SiO<sub>2</sub> nanoparticles have been used to construct ECL sensor for DNA analysis<sup>28,29</sup>, immunoassay<sup>30,31</sup>, cell test<sup>32,33</sup> and so on<sup>34-36</sup>. Since luminophore itself produce low ECL signal, co-reactant such as tripropylamine (TPA) is usually added to the ECL system to enhance the ECL intensity and improve the analytical performance. However, adding co-reactant might lead to a more complex assay system and increase the analytical steps to some extent<sup>37</sup>. Therefore, self-enhanced ECL composite was developed to greatly enhance the ECL signal and simplify

<sup>1</sup>State Key Laboratory of Electroanalytical Chemistry, Changchun Institute of Applied Chemistry, Chinese Academy of Sciences, Changchun 130022, China. <sup>2</sup>University of the Chinese Academy of Sciences, Beijing 100049, China. <sup>3</sup>National Engineering Laboratory for AIDS Vaccine, School of Life Sciences, Jilin University, Changchun 130012, China. Correspondence and requests for materials should be addressed to T.Y. (email: youty@ciac.ac.cn)

the analysis process at the same time. Self-enhanced ECL composite made luminophore and its co-reactant exist in the same composite. In this way, the electron-transfer distance between the luminophore and its co-reactant was shortened and the luminous efficiency could be greatly enhanced<sup>38</sup>. So far, several self-enhanced ECL composites have been proposed and excellent results were obtained<sup>38–41</sup>. For example, Zhuo *et al.* linked Ru(II) with the co-reactant poly(ethylenimine) (PEI) to prepare a self-enhance ECL composite of Ru(II)-PEI and it was used to build an immunosensor for the analysis of apurinic/aprimidinic Endonuclease 1<sup>39</sup>. Wang *et al.* immobilized Ru(II) with the co-reactant polyamidoamine dendrimer (PAMAM) on palladium nanowires and used the self-enhance composite to construct carcinoembryonic antigen (CEA) immunosensor<sup>40</sup>. To further expand the application of the simple and sensitive self-enhanced ECL sensor, preparing new and efficient self-enhanced composite is great important.

Herein, we prepared a novel self-enhanced ECL composite by simply combining PEI with Ru-SiO<sub>2</sub> nanoparticles for the first time, and the obtained hollow Ru-SiO<sub>2</sub>@PEI nanoparticles were used to build an ECL immunosensor for the analysis of NSE. During the interaction, PEI assembled on the surface of the Ru-SiO<sub>2</sub> nanoparticles through electrostatic interaction to work as co-reactant to greatly enhance the ECL signal. At the same time, PEI provided an alkaline condition to etched the Ru-SiO<sub>2</sub> to form the hollow Ru-SiO<sub>2</sub>@PEI nanoparticles with porous shell, which was beneficial for the reaction between PEI and Ru(bpy)<sub>3</sub><sup>2+</sup>. Since a large amount of Ru(bpy)<sub>3</sub><sup>2+</sup> and its co-reactant were loaded in the composite at the same time, strong ECL signal was produced. The proposed immunosensor based on the self-enhanced ECL composites showed wide linear range and low detection limit for NSE. The analytical results were consistent with those obtained from the enzyme-linked immunosorbent assay (ELISA) method when the immunosensor was used for the detection of NSE in clinical human serum. The proposed method showed great promise for the NSE analysis in clinical samples.

## Materials and Reagents

Neuron-specific enolase (NSE), NSE antibody (anti-NSE), NSE ELISA kits and Carcinoembryonic antigen (CEA) were purchased from Linc-Bio Science Co. Ltd (Shanghai, China). Triton X-100, bovine serum albumin (BSA), and alpha fetoprotein (AFP) were supplied by Beijing Dingguo Biotechnology Co., Ltd. (Beijing, China). Tetraethyl orthosilicate (TEOS), Tris (2, 2-bipyridyl) dichlororuthenium(II) hexahydrate (Ru(bpy)<sub>3</sub>Cl<sub>2</sub>·6H<sub>2</sub>O), Poly(ethylenimine) (PEI) and HAuCl<sub>4</sub> were bought from Aldrich. Cyclohexane and ammonium hydroxide (25–28 wt%) were supplied by Beijing Chemical Reagent Factory (Beijing, China). 1-hexanol was offered by Sinopharm Chemical Reagent Co. Ltd (Shanghai, China). Na<sub>2</sub>HPO<sub>4</sub> and NaH<sub>2</sub>PO<sub>4</sub> were used to prepare phosphate buffer solutions (PBS). Washing buffer was 0.05% (w/v) Tween-20 in 0.01 M PBS (pH 7.4). All aqueous solutions in the experiments were prepared with doubly distilled water. Human serum samples were obtained from First Affiliated Hospital of Jilin University. Use of serum samples was approved by First Affiliated Hospital of Jilin University. All experiments were performed in accordance with the approved guidelines and regulations. Informed consent was obtained from all subjects.

**Apparatus.** MPI-E ECL analyzer (XiAn Remax Electronic Science & Technology Co. Ltd., China) was used to record the ECL responses. A voltage of 800 V was supplied to the photomultiplier tube (PMT). CV behaviors were measured on a CHI832 voltammetric analyzer (Shanghai Chenhua Apparatus Inc., China). Modified GCE electrode, a platinum wire and an Ag/AgCl (saturated KCl) electrode were used as working electrode, counter electrode and reference electrode, respectively. UV-visible spectra were recorded on Cary 50 UV-vis spectrophotometer (Varian, America). AUTOLAB PGSTAT302N was used to record the electrochemical impedance Spectroscopy (EIS). Transmission electron microscopy (TEM) was conducted using a JEOL JEM-1011 electron microscope.

**Preparation of Ru-SiO<sub>2</sub>@PEI nanoparticles.** Firstly, Ru-SiO<sub>2</sub> nanoparticles were prepared according to a previous literature<sup>42</sup>. Briefly, 7.08 mL of TritonX-100, 7.2 mL of 1-hexanol, 30 mL of cyclohexane and 1.36 mL of water were mixed together to form a homogeneous solution under stirring. Then, 320 μL of 0.1 M Ru(bpy)<sub>3</sub><sup>2+</sup> aqueous solution and 400 μL of TEOS were added. Afterwards, 240 μL of NH<sub>4</sub>OH was added to initiate the polymerization reaction. After reacting for 24 hours, the Ru-SiO<sub>2</sub> nanoparticles were isolated by adding acetone to the mixture. Followed by washing with ethanol and water for several times to remove any surfactant molecules, the nanoparticles were suspended in 15 mL water for further experiments.

Ru-SiO<sub>2</sub>@PEI nanoparticles were synthesized by adding 10 mL of 20 mg mL<sup>-1</sup> PEI to 10 mL of 0.5 mg mL<sup>-1</sup> Ru-SiO<sub>2</sub> nanoparticles solution and stirred for 12 hours. After centrifuging and washing with water for several times, Ru-SiO<sub>2</sub>@PEI nanoparticles were obtained. The nanoparticles for different PEI concentration or reaction time were prepared in the same way.

**Fabrication of the ECL immunosensor.** The fabrication process of the immunosensor was exhibited in Fig. 1. Firstly, GCE (3 mm) was polished with 0.3 μm and 0.05 μm alumina powders to obtain mirror-like surface, followed by sonicating in ethanol and water thoroughly and drying at room temperature. 5 μL of Ru-SiO<sub>2</sub>@PEI nanoparticles was dropped onto the pretreated GCE and dried in air. To avoid the ECL composite falling down from the electrode, 2 μL of Nafion was dropped on the electrode to form a Nafion film. Then, the modified electrode was immersed into HAuCl<sub>4</sub> (1%) solution and electrochemical deposited with constant potential of -0.2 V for 15 s to obtain Au NPs layer. Subsequently, anti-NSE was immobilized on the electrode by soaking the electrode in 80 μL of anti-NSE solution at 4 °C for 24 h. Thereafter, the electrode was immersed in 80 μL of 1% BSA at 37 °C for 1 h to block the nonspecific binding sites. Finally, the electrode was incubated with 80 μL of NSE solution at 37 °C for 80 min to capture the NSE through the interaction between the antibody and antigen. After each modified step, the modified electrode was thoroughly washed with washing buffer to remove the physically absorbed species. ECL response of the proposed immunosensor was investigated in 0.1 M PBS (pH 7.5).

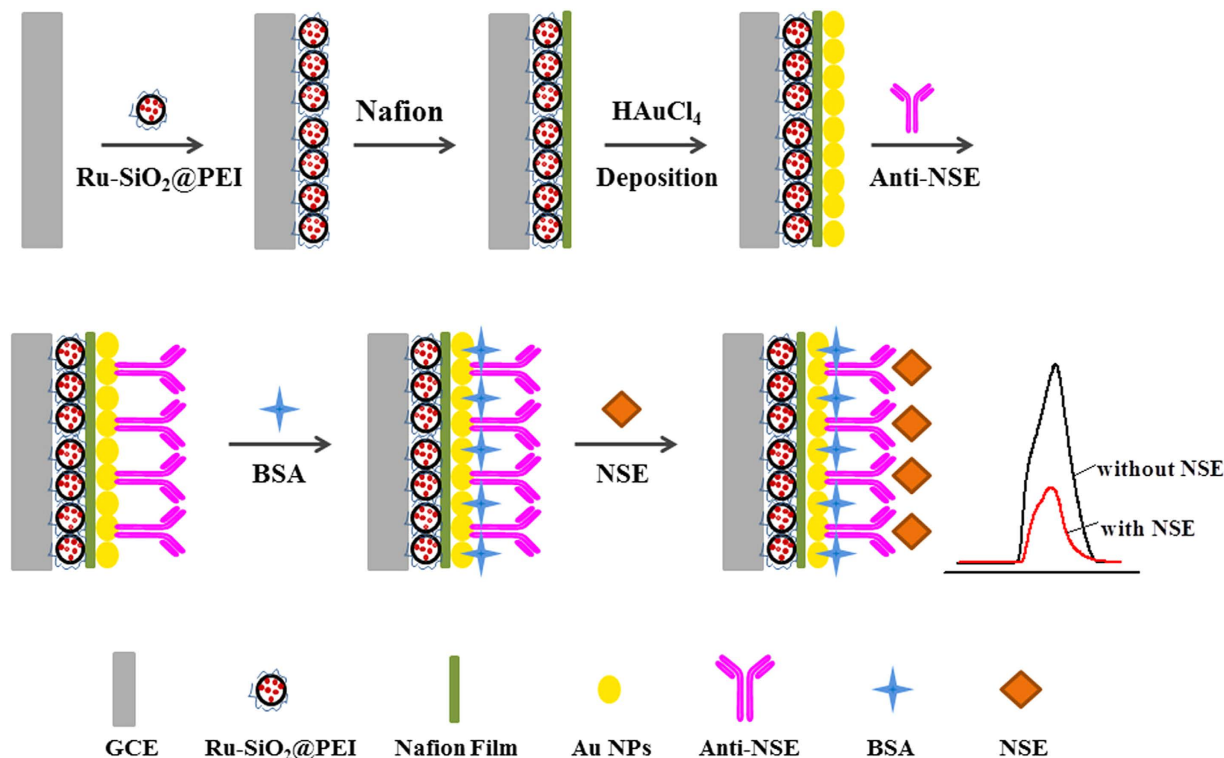


**Figure 1.** The fabrication process of the proposed immunosensor.

## Results and Discussion

**Characteristics of Ru-SiO<sub>2</sub> and Ru-SiO<sub>2</sub>@PEI nanoparticles.** As shown in Fig. 2A, the prepared Ru-SiO<sub>2</sub> nanoparticles were spherical and uniform in size. When the Ru-SiO<sub>2</sub> nanoparticles suspension was combined with PEI solution, hollow Ru-SiO<sub>2</sub>@PEI nanoparticles were obtained (Fig. 2F). To understand the formation process of the hollow structure, Ru-SiO<sub>2</sub>@PEI nanoparticles with different reaction time were investigated (Fig. 2B–F). As can be seen, when the reaction time was 0.5 h, many small pores produced inside the nanoparticles. With the increase of reaction time, these small pores merged into a larger cavity and eventually generated the hollow nanoparticles. It's well-known that SiO<sub>2</sub> could be etched in alkaline solution by breaking the Si-O-Si bond<sup>43</sup>. During the interaction between Ru-SiO<sub>2</sub> nanoparticles and PEI, on one hand, PEI could assemble on the surface of Ru-SiO<sub>2</sub> nanoparticles through electrostatic interaction. As shown in Figure S1, the Ru-SiO<sub>2</sub> nanoparticles were negatively charged while the Ru-SiO<sub>2</sub>@PEI nanoparticles were positively charged, which suggested that PEI assembled on the surface of Ru-SiO<sub>2</sub> nanoparticles successfully. On the other hand, the presence of protonated amine groups in the PEI chain provided an alkaline condition, which resulted in the etching of Ru-SiO<sub>2</sub> nanoparticles<sup>44</sup>. Since the PEI on the surface of the Ru-SiO<sub>2</sub> nanoparticles could work as protecting agent to prevent the dissolution of the Si-O-Si bond near the outer surface<sup>44,45</sup>, as a result, the interior of the Ru-SiO<sub>2</sub> was etched and eventually formed the hollow Ru-SiO<sub>2</sub>@PEI nanoparticles. In addition, the nitrogen adsorption-desorption isotherm measurement showed that the surface areas increased from 97.8 to 161.9 m<sup>2</sup> g<sup>-1</sup> when the Ru-SiO<sub>2</sub> nanoparticles interacted with PEI to form the hollow Ru-SiO<sub>2</sub>@PEI nanoparticles. From the pore distribution curve measured by the BJH method (Figure S2), we can see that the pore diameter of Ru-SiO<sub>2</sub> nanoparticles is about 2 nm in average. While for the Ru-SiO<sub>2</sub>@PEI nanoparticles, the ratio of some larger pores with average diameter about 4 nm increased due to the etching of Ru-SiO<sub>2</sub> nanoparticles. Moreover, when different concentrations of PEI were interacted with Ru-SiO<sub>2</sub> nanoparticles for 12 h, the hollow-structured nanoparticles were obtained successfully (Figure S3), indicating that the concentration of PEI in the studied range has little effect on the formation of the hollow structure.

The UV-vis absorption spectra of Ru-SiO<sub>2</sub> and Ru-SiO<sub>2</sub>@PEI nanoparticles were shown in Fig. 3. Two obvious peaks appeared at about 287 nm and 457 nm in the spectrum of Ru-SiO<sub>2</sub> nanoparticles, which were assigned to ligand-centered transitions and metal-to-ligand charge transfer (MLCT) of Ru(bpy)<sub>3</sub><sup>2+</sup> molecule, respectively<sup>46</sup>. This indicated that Ru(bpy)<sub>3</sub><sup>2+</sup> molecules were successfully encapsulated in the Ru-SiO<sub>2</sub> nanoparticles. After reacting with PEI to form the hollow Ru-SiO<sub>2</sub>@PEI nanoparticles, there was no obvious change in the UV spectrum, which suggested that the Ru(bpy)<sub>3</sub><sup>2+</sup> molecules still maintained in the Ru-SiO<sub>2</sub>@PEI nanoparticles.

**Electrochemistry and ECL behavior.** 5 μL of 0.5 mg mL<sup>-1</sup> Ru-SiO<sub>2</sub>@PEI nanoparticles were coated on the GCE electrode (Ru-SiO<sub>2</sub>@PEI/GCE) and the modified electrode was scanned in 0.1 M PBS (pH = 7.5). The cyclic voltammograms (CV) and ECL-potential curve (Fig. 4A) showed that the characteristic redox of Ru(bpy)<sub>3</sub><sup>2+</sup> with an oxidation peak appeared near 1.1 V (curve a) and high ECL signal was produced (curve b), which indicated that Ru(bpy)<sub>3</sub><sup>2+</sup> molecules in the Ru-SiO<sub>2</sub>@PEI nanoparticles still maintained its properties. The luminescence



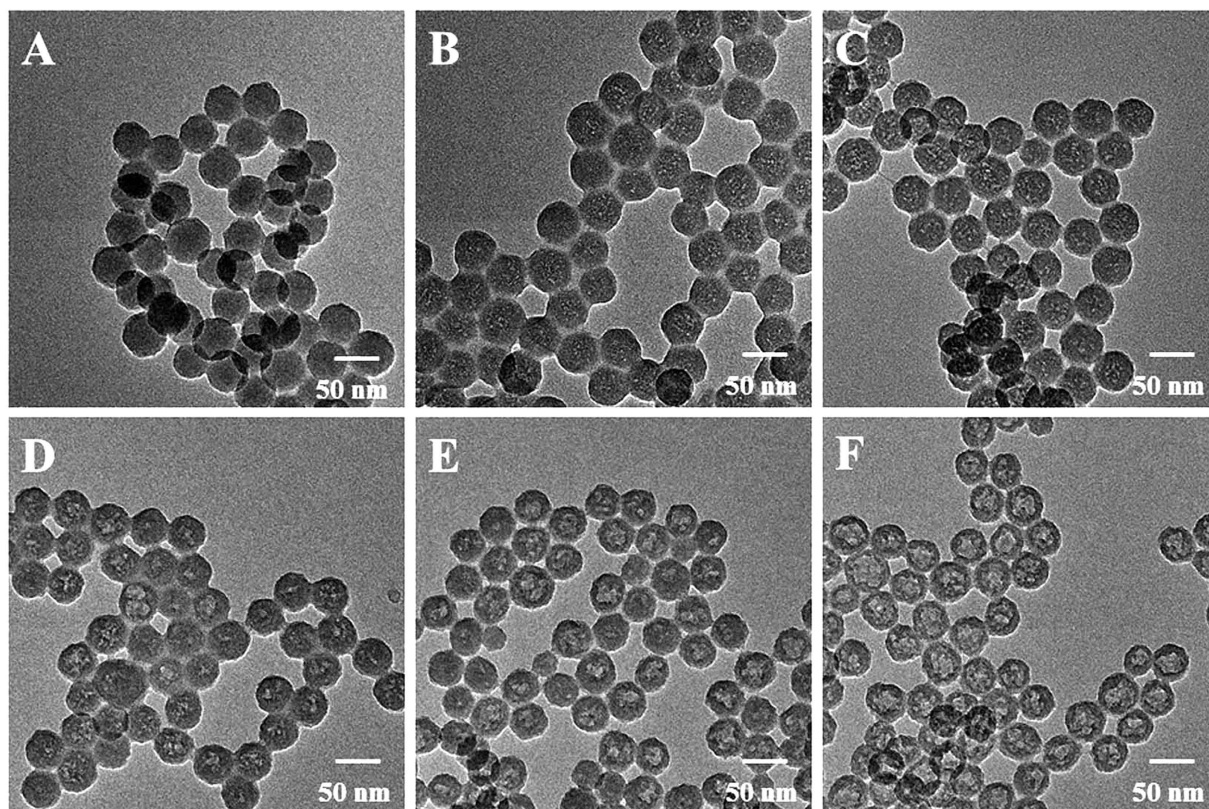


**Figure 2.** TEM images of (A) Ru-SiO<sub>2</sub> nanoparticles and Ru-SiO<sub>2</sub>@PEI nanoparticles with the reaction time of (B) 0.5 h, (C) 2 h, (D) 6 h, (E) 9 h and (F) 12 h.

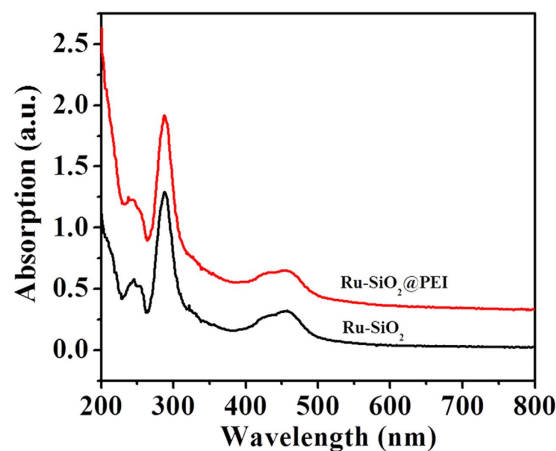


**Figure 3.** UV-vis absorption spectra of Ru-SiO<sub>2</sub> and Ru-SiO<sub>2</sub>@PEI nanoparticles.

began around 1.0 V and reached to its maximum value at 1.1 V, which was consistent with the oxidation potential of Ru(bpy)<sub>3</sub><sup>2+</sup>, suggesting that the oxidation of Ru(bpy)<sub>3</sub><sup>2+</sup> played an important role in the process of ECL. In addition, compared with Ru-SiO<sub>2</sub> nanoparticles modified electrode (Ru-SiO<sub>2</sub>/GCE) (Fig. 4B, curve a), the ECL intensity of Ru-SiO<sub>2</sub>@PEI/GCE increased about 25 times (Fig. 4B, curve b). This great signal enhancement can be attributed to that PEI with amine groups could work as co-reactant to enhance the ECL of Ru(bpy)<sub>3</sub><sup>2+</sup><sup>38</sup>. Furthermore, when the Ru-SiO<sub>2</sub>/GCE was scanned in 0.1 M PBS (pH 7.5) containing of 20 mg mL<sup>-1</sup> PEI (Fig. 4B, curve c), the ECL intensity was enhanced about 5 times, which indicated that PEI could indeed enhance the ECL of Ru(bpy)<sub>3</sub><sup>2+</sup>. However, the signal enhancement is still much lower than that of Ru-SiO<sub>2</sub>@PEI/GCE. This can be explained that both a large amount of Ru(bpy)<sub>3</sub><sup>2+</sup> and its co-reactant PEI were loaded in the Ru-SiO<sub>2</sub>@PEI nanoparticles at the same time so that the electron-transfer distance was shortened, by which the luminous efficiency was enhanced and resulted in the high ECL response<sup>36</sup>. In a word, the prepared Ru-SiO<sub>2</sub>@PEI nanoparticles produced the highest ECL signal by self-enhancement. According to the electrochemistry and ECL behaviors of

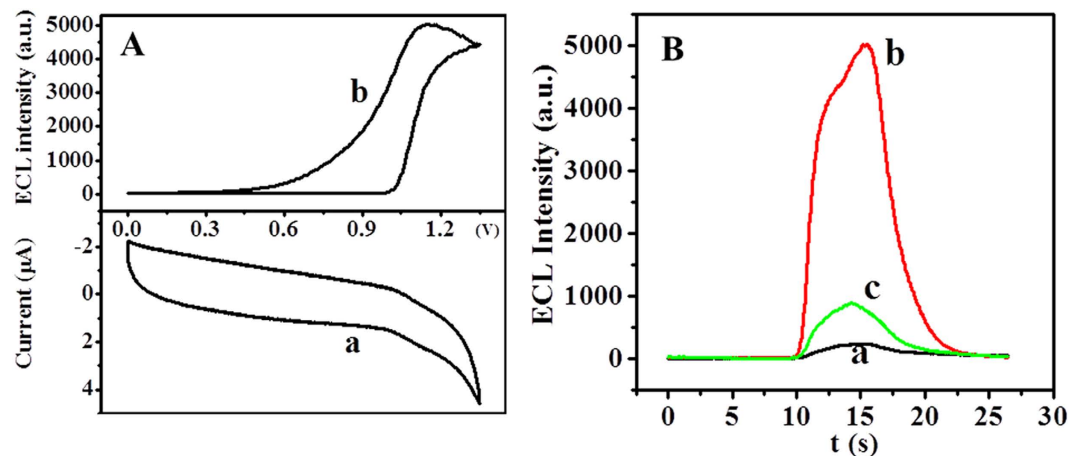
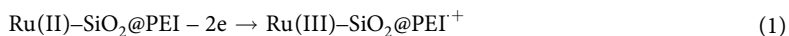


**Figure 4.** (A) Cyclic voltammograms (a) and ECL–potential curve (b) of Ru-SiO<sub>2</sub>@PEI/GCE in 0.1 M PBS (pH 7.5). (B) ECL response of (a) Ru-SiO<sub>2</sub>/GCE, (b) Ru-SiO<sub>2</sub>@PEI/GCE in 0.1 M PBS (pH 7.5) and (c) Ru-SiO<sub>2</sub>/GCE in 0.1 M PBS (pH 7.5) containing of 20 mg mL<sup>-1</sup> PEI. Scan rate: 100 mV s<sup>-1</sup>. Scan potential: 0–1.35 V.

the Ru-SiO<sub>2</sub>@PEI nanoparticles and the previous reports<sup>38,39</sup>, we proposed the possible ECL mechanism of the Ru-SiO<sub>2</sub>@PEI nanoparticles as below:



**Characterization of the immunosensor.** As indicated above, Ru-SiO<sub>2</sub>@PEI nanoparticles could produce high ECL signal without any extra addition. Thus, we constructed a self-enhanced ECL immunosensor for the analysis of NSE. And then, the fabrication process of the immunosensor was firstly investigated. Figure 5A showed the ECL responses of each step in 0.1 M PBS (curve a). When Ru-SiO<sub>2</sub>@PEI nanoparticles were coated on GCE, great ECL signal was produced (Fig. 5A, curve b). After electrodeposition of Au NPs on the electrode, the ECL intensity was enhanced (Fig. 5A, curve c), since the good conductivity of Au NPs could increase the electron transfer on the electrode and amplified the ECL signal. When anti-NSE was assembled on the electrode via the interaction between the Au NPs and the amino groups of anti-NSE, ECL intensity decreased about 1800 a.u. (Fig. 5A, curve d), which was attributed to that the electronically insert feature of antibody hindered the electron transfer on the electrode and lead to the decrease in ECL response. In addition, ECL signal decreased again after BSA blocked the non-specific site (Fig. 5A, curve e). Finally, when NSE antigen was immobilized on the electrode through the interaction between antigen and antibody, ECL intensity decreased further (Fig. 5A, curve f). These results indicated that each step was constructed successfully, and also suggested that the proposed immunosensor could be used to highly sensitive detection of target antigen based on the decrease of the ECL signal.

CVs responses of each step in 0.1 M KCl containing 5.0 mM [Fe(CN)<sub>6</sub>]<sup>3-/4-</sup> were displayed in Fig. 5B. The bare GCE exhibited a pair of reversible redox peaks (Fig. 5B, curve a). After Ru-SiO<sub>2</sub>@PEI nanoparticles were coated on the electrode, the peak current decreased due to the poor conductivity of Ru-SiO<sub>2</sub>@PEI nanoparticles (Fig. 5B, curve b). Subsequently, the peak current obviously increased when conductive Au NPs were electrodeposited on the electrode (Fig. 5B, curve c). However, the peak current decreased consecutively when the electrode assembled anti-NSE, BSA and NSE successively (Fig. 5B, curve d–f), owing to that the electron insulated protein molecules blocked the electron transfer on the electrode surface. At the same time, these changes in CV confirmed that anti-NSE, BSA and NSE were immobilized on the electrode successfully.

Electrochemical impedance spectroscopy (EIS) was also conducted to evaluate the fabrication process of the immunosensor (Fig. 5C). When the low conductivity of Ru-SiO<sub>2</sub>@PEI nanoparticles were coated on GCE, electron transfer resistance (*Ret*) increased (Fig. 5C, curve b), while the electrodeposition of Au NPs resulted in decreased *Ret* (Fig. 5C, curve c). However, *Ret* increased consecutively after the successively immobilization of electron insulated anti-NSE, BSA and NSE on the electrode (Fig. 5C, curve d–f). These results were consistent with ECL and CV response.

**Optimization of experimental parameter.** To obtain good analytical performance, several experimental parameters, including the concentration of Ru-SiO<sub>2</sub>@PEI, the concentration of the anti-NSE, incubation time between antibody and antigen and pH of the detection solution were optimized. Firstly, the effect of Ru-SiO<sub>2</sub>@PEI concentration on the ECL intensity was shown in Figure S4A. The ECL intensity increased with the increase

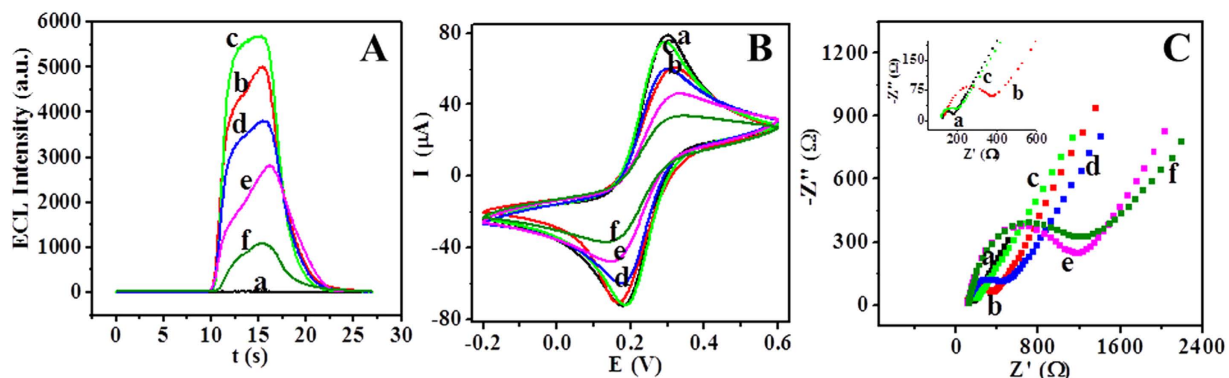


**Figure 5.** (A) ECL, (B) CV and (C) EIS responses of (a) GCE, (b) Ru-SiO<sub>2</sub>@PEI/GCE (c) Au/Ru-SiO<sub>2</sub>@PEI/GCE, (d) anti-NSE/Au/Ru-SiO<sub>2</sub>@PEI/GCE, (e) BSA/anti-NSE/Au/Ru-SiO<sub>2</sub>@PEI/GCE, (f) NSE/BSA/anti-NSE/Au/Ru-SiO<sub>2</sub>@PEI/GCE. The ECL responses were measured in 0.1 M PBS (pH 7.5); Scan rate: 100 mV s<sup>-1</sup>. Scan potential: 0~1.35 V. CV and EIS were conducted in 0.1 M KCl solution containing of 5.0 mM [Fe(CN)<sub>6</sub>]<sup>3-/4-</sup>.

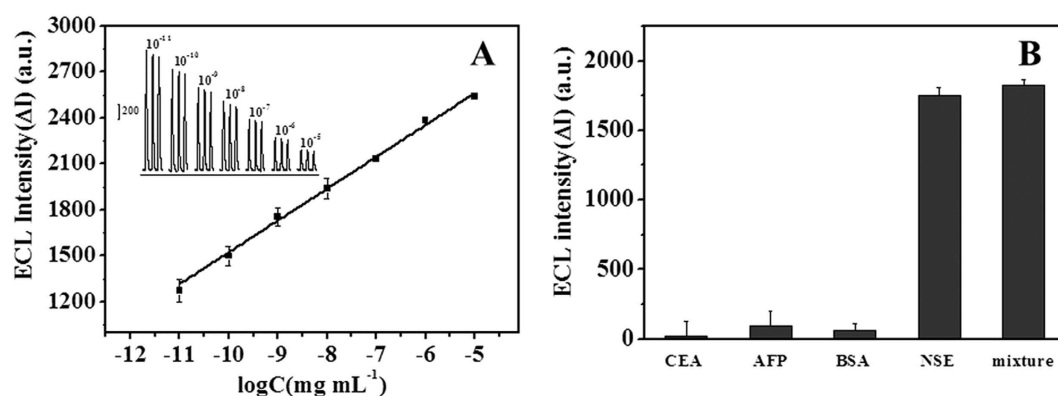


**Figure 6.** (A) Calibration curve of decrease value of ECL intensity ( $\Delta I$ ) to logarithmic NSE concentration. Inset: ECL-time curves of the immunosensor incubating with  $1.0 \times 10^{-11}$  mg mL<sup>-1</sup>,  $1.0 \times 10^{-10}$  mg mL<sup>-1</sup>,  $1.0 \times 10^{-9}$  mg mL<sup>-1</sup>,  $1.0 \times 10^{-8}$  mg mL<sup>-1</sup>,  $1.0 \times 10^{-7}$  mg mL<sup>-1</sup>,  $1.0 \times 10^{-6}$  mg mL<sup>-1</sup> and  $1.0 \times 10^{-5}$  mg mL<sup>-1</sup> of NSE. (B) ECL responses of the proposed immunosensor incubating with  $2.0 \times 10^{-8}$  mg mL<sup>-1</sup> of CEA, AFP, BSA,  $1.0 \times 10^{-9}$  mg mL<sup>-1</sup> of NSE and their mixture. The ECL response was determined in 0.1 M PBS (pH 7.5); Scan rate: 100 mV s<sup>-1</sup>. Scan potential: 0~1.35 V.

of Ru-SiO<sub>2</sub>@PEI concentration from 0.1 to 0.5 mg mL<sup>-1</sup>, and it began to decrease thereafter. This was due to that with the increase concentration of Ru-SiO<sub>2</sub>@PEI, more ECL molecules were immobilized on the electrode and produced high ECL signal. However, the ECL emission might be absorbed or scattered by too much ECL molecules<sup>42</sup>. Therefore, 0.5 mg mL<sup>-1</sup> of Ru-SiO<sub>2</sub>@PEI was used to construct the sensor.

The concentration of the anti-NSE during the construction of the immunosensor was optimized. As shown in Figure S4B, the ECL decreased with the increase of the concentration of the anti-NSE from 0.1 to 1  $\mu$ g mL<sup>-1</sup>, and it began to stabilize with higher concentration, which indicated the saturated immobilization of anti-NSE on the electrode. Thus, we used 1  $\mu$ g mL<sup>-1</sup> anti-NSE to build the immunosensor.

The incubation time between antigen and antibody was an important factor influencing the ECL signal. As indicated in Figure S4C, the ECL intensity decreased with longer incubation time and reached a plateau after 80 min, which showed a saturated binding of NSE on the electrode. Thus, 80 min of incubation time was selected for the sensor.

In addition, pH value effect was also investigated. As exhibited in Figure S4D, the ECL signal increased with pH value from 6.0 to 7.5 and it began to decrease with higher pH value. According to the ECL mechanism of the system, higher pH value was favorable for the deprotonation which resulted in high ECL signal. However, too high pH value might lead to decomposition of some species<sup>42</sup>. Hence, pH 7.5 was used in the experiment.

**Analytical performance of the immunosensor.** The analytical performance of the immunosensor was investigated by incubating the immunosensor in NSE solution with different concentrations under the optimal conditions. As shown in Fig. 6A, the ECL intensity decreased with higher concentration of NSE, which due to that the electron insulated NSE hindered the electron transfer on the electrode. The decrease value of ECL intensity ( $\Delta I = I_0 - I$ ,  $I_0$  stands for the ECL intensity without NSE and  $I$  is the ECL intensity with NSE.) was proportional to the logarithm of NSE concentration in the range from  $1.0 \times 10^{-11}$  to  $1.0 \times 10^{-5}$  mg mL<sup>-1</sup> with a detection limit



Method	Linear range (mg mL <sup>-1</sup> )	Detection limit (mg mL <sup>-1</sup> )	Reference
Label-less immunoassay based upon an alternating current impedance protocol	$1.0 \times 10^{-9} - 5.0 \times 10^{-8}$	$5.0 \times 10^{-10}$	4
Multiplexing determination by immunocapture LC-MS/MS		$2.1 \times 10^{-7}$	10
Electrocatalytic oxidation of DA based on NiHCFNPs to amplify electrochemical signal	$1.0 \times 10^{-9} - 1.0 \times 10^{-4}$	$3.0 \times 10^{-10}$	1
Simultaneous detection of two lung cancer biomarkers using dual-color fluorescence quantum dots	$3.0 \times 10^{-6} - 1.0 \times 10^{-4}$	$1.0 \times 10^{-6}$	6
Photoelectrochemical immunosensor based on ZnCdHgSe quantum dots/polymerized ionic liquid hybrid film	$1.0 \times 10^{-9} - 1.0 \times 10^{-4}$	$2.0 \times 10^{-10}$	11
Microfluidic competitive enzyme immunoassay based on chemiluminescence resonance energy transfer	$4.2 \times 10^{-7} - 4.4 \times 10^{-5}$	$2.1 \times 10^{-7}$	8
Fluorescent and electrochemical detection based on CaCO <sub>3</sub> /AuNCs hybrid spheres	$5.0 \times 10^{-9} - 1.0 \times 10^{-6}$ $5.0 \times 10^{-10} - 2.0 \times 10^{-6}$	$2.0 \times 10^{-9}$ $1.0 \times 10^{-10}$	7
ECL immunosensor based on Ru-SiO <sub>2</sub> @PEI nanoparticles	$1.0 \times 10^{-11} - 1.0 \times 10^{-5}$	$1.0 \times 10^{-11}$	This work

**Table 1. Comparison of analytical performance of proposed immunosensor with other methods.**

Sample	ECL immunosensor (ng mL <sup>-1</sup> , n = 6)	ELISA (ng mL <sup>-1</sup> )	Relative Standard Deviation (%)
1	39.27	39.95	-1.72
2	50.05	47.27	5.87
3	100.55	93.01	8.11
4	110.43	112.87	-2.16

**Table 2. Assay results of NSE level in clinical serum samples using the proposed ECL immunosensor and ELISA method.**

of  $1.0 \times 10^{-11}$  mg mL<sup>-1</sup>. The linear regression equation is  $\Delta I = 207.51 \times \log C_{\text{NSE}} + 3599.03$  with a correlation coefficient of 0.992. The comparison of analytical performance of the proposed immunosensor with previous reports was listed in Table 1. It can be found that the present work showed lower detection limit and wider linear range over other approaches.

The excellent analytical performances of the proposed method were attributed to the high ECL intensity produced by the self-enhanced Ru-SiO<sub>2</sub>@PEI nanoparticles. Since both a large amount of Ru(bpy)<sub>3</sub><sup>2+</sup> and its co-reactant PEI were loaded on the Ru-SiO<sub>2</sub>@PEI nanoparticles at the same time, the ECL signal was greatly amplified and resulted in the good analytical performances.

AFP, CEA and BSA were used as interference agents to evaluate the specificity of the immunosensor. As shown in Fig. 6B, the ECL responses of pure AFP, CEA and BSA were negligible compared with that of NSE. What's more, the ECL signal of the mixture of AFP, CEA, BSA and NSE was similar to that of the NSE. These results demonstrated that the proposed immunosensor possessed good specificity for the analysis of NSE. In addition, the relative standard deviation (RSD) for five different immunosensors was 4.4%, which indicated good fabrication reproducibility. Furthermore, the RSD for ten continuous scan of an immunosensor was 5.4% and the ECL signal could still maintain 84% of the initial intensity after one month, which suggested good stability of the immunosensor.

**Analysis of NSE in clinical human serum.** To investigate the practical application of the proposed immunosensor, it was used to the detection of NSE in clinical human serum samples. The assay results were compared with the reference value obtained by the commercial ELISA kits. As shown in Table 2, the relative deviation between the two methods was range from -2.16 to 8.11%, which indicated that the developed immunosensor had potential application in the analysis of NSE in clinical samples.

## Conclusion

A novel self-enhanced electrochemiluminescence immunosensor for the analysis of NSE was developed based on hollow Ru-SiO<sub>2</sub>@PEI nanoparticles. The unique structure of Ru-SiO<sub>2</sub>@PEI nanoparticles as well as high loading of Ru(bpy)<sub>3</sub><sup>2+</sup> and PEI greatly enhanced the luminous efficiency and resulted in high ECL intensity. The developed immunosensor exhibited seven orders of magnitude linear range and  $1.0 \times 10^{-11}$  mg mL<sup>-1</sup> detection limit for the analysis of NSE. The immunosensor was successfully used to the analysis of clinical human serum samples, and the results are consistent with that obtained by the commercial ELISA kits. The proposed method provides a promising alternative for NSE antigen analysis in clinical samples.

## References

- Han, J., Zhuo, Y., Chai, Y. Q., Yuan, Y. L. & Yuan, R. Novel electrochemical catalysis as signal amplified strategy for label-free detection of neuron-specific enolase. *Biosens. Bioelectron.* **31**, 399–405 (2012).
- Oremek, G. M., Sauer-Eppel, H. & Bruzdziak, T. H. Value of tumour and inflammatory markers in lung cancer. *Anticancer Res.* **27**, 1911–1915 (2007).
- Lu, W. *et al.* An electrochemical immunosensor for simultaneous multiplexed detection of two lung cancer biomarkers using Au nanoparticles coated resin microspheres composed of l-tryptophan and caffeic acid. *Ionics* **21**, 1141–1152 (2015).

4. Barton, A. C., Davis, F. & Higson, S. P. J. Labelless immunosensor assay for the stroke marker protein neuron specific enolase based upon an alternating current impedance protocol. *Anal. Chem.* **80**, 9411–9416 (2008).
5. Wang, L., Liu, N. & Ma, Z. Novel gold-decorated polyaniline derivatives as redox-active species for simultaneous detection of three biomarkers of lung cancer. *J. Mater. Chem. B* **3**, 2867–2872 (2015).
6. Li, H., Cao, Z., Zhang, Y., Lau, C. & Lu, J. Simultaneous detection of two lung cancer biomarkers using dual-color fluorescence quantum dots. *Analyst* **136**, 1399–1405 (2011).
7. Peng, J. *et al.* Calcium carbonate-gold nanocluster hybrid spheres: synthesis and versatile application in immunoassays. *Chem. -Eur. J.* **18**, 5261–5268 (2012).
8. Yang, T., Vdovenko, M., Jin, X., Sakharov, I. Y. & Zhao, S. Highly sensitive microfluidic competitive enzyme immunoassay based on chemiluminescence resonance energy transfer for the detection of neuron-specific enolase. *Electrophoresis* **35**, 2022–2028 (2014).
9. Fu, X. *et al.* Chemiluminescence enzyme immunoassay using magnetic nanoparticles for detection of neuron specific enolase in human serum. *Anal. Chim. Acta.* **722**, 114–118 (2012).
10. Torsetnes, S. B. *et al.* Multiplexing determination of small cell lung cancer biomarkers and their isovariants in serum by immunocapture LC-MS/MS. *Anal. Chem.* **86**, 6983–6992 (2014).
11. Yu, X. *et al.* White-light-exciting, layer-by-layer-assembled ZnCdHgSe quantum dots/polymerized ionic liquid hybrid film for highly sensitive photoelectrochemical immunosensing of neuron specific enolase. *Anal. Chem.* **87**, 4237–4244 (2015).
12. Cheng, S., Hideshima, S., Kuroiwa, S., Nakanishi, T. & Osaka, T. Label-free detection of tumor markers using field effect transistor (FET)-based biosensors for lung cancer diagnosis. *Sens. Actuators, B* **212**, 329–334 (2015).
13. Fu, X., Xu, K., Ye, J., Chen, J. & Feng, X. Glucoamylase-labeled nanogold flowers for *in situ* enhanced sensitivity of a glucometer-based enzyme immunoassay. *Anal. Methods* **7**, 507–512 (2015).
14. Raluca-Ioana, S. S., Ionela, R. C., Carmen, C. S. & Marius, B. Nanostructured materials detect epidermal growth factor receptor, neuron specific enolase and carcinoembryonic antigen. *Nanoscale* **7**, 15689–15694 (2015).
15. Jiang, D. *et al.* Anchoring AgBr nanoparticles on nitrogen-doped graphene for enhancement of electrochemiluminescence and radical stability. *Chem. Commun.* **51**, 4451–4454 (2015).
16. Du, X. *et al.* An ON1-OFF-ON2 electrochemiluminescence response: combining the intermolecular specific binding with a radical scavenger. *Chem. Commun.* **51**, 11236–11239 (2015).
17. Hu, T., Li, T., Yuan, L., Liu, S. & Wang, Z. Anodic electrogenerated chemiluminescence of quantum dots: size and stabilizer matter. *Nanoscale* **4**, 5447–5453 (2012).
18. Hu, T., Liu, X., Liu, S., Wang, Z. & Tang, Z. Toward understanding of transfer mechanism between electrochemiluminescent dyes and luminescent quantum dots. *Anal. Chem.* **86**, 3939–3946 (2014).
19. Li, H. *et al.* A nanobody-based electrochemiluminescent immunosensor for sensitive detection of human procalcitonin. *Analyst* **139**, 3718–3721 (2014).
20. Gao, F., Lei, J. & Ju, H. Label-free surface-enhanced raman spectroscopy for sensitive DNA detection by DNA-mediated silver nanoparticle growth. *Anal. Chem.* **85**, 11788–11793 (2013).
21. Lou, J., Liu, S., Tu, W. & Dai, Z. Graphene quantum dots combined with endonuclease cleavage and bidentate chelation for highly sensitive electrochemiluminescent DNA biosensing. *Anal. Chem.* **87**, 1145–1151 (2015).
22. Zhou, J. *et al.* Electrochemiluminescence imaging for parallel single-cell analysis of active membrane cholesterol. *Anal. Chem.* **87**, 8138–8143 (2015).
23. Xia, H., Li, L., Yin, Z., Hou, X. & Zhu, J. Biobar-coded gold nanoparticles and DNAzyme-based dual signal amplification strategy for ultrasensitive detection of protein by electrochemiluminescence. *ACS Appl. Mater. Interfaces* **7**, 696–703 (2015).
24. Huang, T., Meng, Q. & Jie, G. Silver nanowires-based signal amplification for CdSe quantum dots electrochemiluminescence immunoassay. *Biosens. Bioelectron.* **66**, 84–88 (2015).
25. Wu, L., Ma, C., Zheng, X., Liu, H. & Yu, J. Paper-based electrochemiluminescence origami device for protein detection using assembled cascade DNA-carbon dots nanotags based on rolling circle amplification. *Biosens. Bioelectron.* **68**, 413–20 (2015).
26. Xu, Y., Yin, X. B., He, X. W. & Zhang, Y. K. Electrochemistry and electrochemiluminescence from a redox-active metal-organic framework. *Biosens. Bioelectron.* **68**, 197–203 (2015).
27. Yu, Y., Lu, C. & Zhang, M. Gold nanoclusters@Ru(bpy)(3)(2+)-layered double hydroxide ultrathin film as a cathodic electrochemiluminescence resonance energy transfer probe. *Anal. Chem.* **87**, 8026–8032 (2015).
28. Wu, M. S., He, L. J., Xu, J. J. & Chen, H. Y. RuSi@Ru(bpy)(3)(2+)/Au@Ag2S nanoparticles electrochemiluminescence resonance energy transfer system for sensitive DNA detection. *Anal. Chem.* **86**, 4559–4565 (2014).
29. Bae, S. W. *et al.* A doubly signal-amplified DNA detection method based on pre-complexed [Ru(bpy)(3)](2+)-doped silica nanoparticles. *Chem. -Eur. J.* **16**, 11572–11575 (2010).
30. Shao, K. *et al.* Stretch-stowage-growth strategy to fabricate tunable triply-amplified electrochemiluminescence immunosensor for ultrasensitive detection of pseudorabies virus antibody. *Anal. Chem.* **86**, 5749–5757 (2014).
31. Li, J., Guo, L. R., Gao, W., Xia, X. H. & Zheng, L. M. Enhanced electrochemiluminescence efficiency of Ru(II) derivative covalently linked carbon nanotubes hybrid. *Chem. Commun.* 7545–7547; doi: 10.1039/B916007H (2009).
32. Wu, Y. *et al.* Signal amplification cytosensor for evaluation of drug-induced cancer cell apoptosis. *Anal. Chem.* **84**, 1894–1899 (2012).
33. Chen, Z., Liu, Y., Wang, Y., Zhao, X. & Li, J. Dynamic evaluation of cell surface N-Glycan expression via an electrogenerated chemiluminescence biosensor based on concanavalin a-integrating gold-nanoparticle-modified Ru(bpy)(3)(2+)-doped silica nanoprobe. *Anal. Chem.* **85**, 4431–4438 (2013).
34. Chen, L. *et al.* A sensitive aptasensor for adenosine based on the quenching of Ru(bpy)(3)(2+)-doped silica nanoparticle ECL by ferrocene. *Chem. Commun.* **46**, 7751–7753 (2010).
35. Jia, T. T. *et al.* Electrogenerated chemiluminescence ethanol biosensor based on alcohol dehydrogenase functionalized Ru(bpy)(3)(2+) doped silica nanoparticles. *Biosens. Bioelectron.* **25**, 263–267 (2009).
36. Lv, X. *et al.* Electrochemiluminescence modified electrodes based on RuSi@Ru(bpy)32+ loaded with gold functionalized nanoporous CO/Co3O4 for detection of mycotoxin deoxynivalenol. *Biosens. Bioelectron.* **70**, 28–33 (2015).
37. Liao, N. *et al.* Reagent less electrochemiluminescent detection of protein biomarker using graphene-based magnetic nanoprobe and poly-L-lysine as co-reactant. *Biosens. Bioelectron.* **45**, 189–194 (2013).
38. Wang, H., He, Y., Chai, Y. & Yuan, R. A super intramolecular self-enhanced electrochemiluminescence immunosensor based on polymer chains grafted on palladium nanocages. *Nanoscale* **6**, 10316–10322 (2014).
39. Zhuo, Y. *et al.* Ultrasensitive apurinic/aprimidinic endonuclease I immunosensing based on self-enhanced electrochemiluminescence of a Ru(II) complex. *Anal. Chem.* **86**, 1053–1060 (2014).
40. Wang, H., Yuan, Y., Chai, Y. & Yuan, R. Self-enhanced electrochemiluminescence immunosensor based on nanowires obtained by a green approach. *Biosens. Bioelectron.* **68**, 72–77 (2015).
41. Zhao, M. *et al.* Triple quenching of a novel self-Enhanced Ru(II) complex by hemin/G-quadruplex DNAzymes and its potential application to quantitative protein detection. *Anal. Chem.* **87**, 7602–7609 (2015).
42. Zhang, L. & Dong, S. Electrogenerated chemiluminescence sensors using Ru(bpy)(3)(2+) doped in silica nanoparticles. *Anal. Chem.* **78**, 5119–5123 (2006).
43. Park, S. J., Kim, Y. J. & Park, S. J. Size-dependent shape evolution of silica nanoparticles into hollow structures. *Langmuir* **24**, 12134–12137 (2008).



44. Zhang, L. *et al.* General route to multifunctional uniform yolk/mesoporous silica shell nanocapsules: a platform for simultaneous cancer-targeted imaging and magnetically guided drug delivery. *Chem. -Eur. J.* **18**, 12512–12521 (2012).
45. Zhang, Q., Zhang, T., Ge, J. & Yin, Y. Permeable silica shell through surface-protected etching. *Nano Lett.* **8**, 2867–2871 (2008).
46. Innocenzi, P., Kozuka, H. & Yoko, T. Fluorescence properties of the Ru(bpy)<sub>3</sub>(2+) complex incorporated in sol-gel-derived silica coating films. *J. Phys. Chem. B* **101**, 2285–2291 (1997).

### Acknowledgements

This work was supported by National Science Foundation of China (21222505, 21475124, 21105098) and China Postdoctoral Science Foundation (2014T70301).

### Author Contributions

L.Z. and T.Y. conceived and designed the experiments. L.Z., J.H. and B.Y. performed the experiments. L.Z., J.H. and T.Y. analyzed the data. L.Z. wrote the first draft of the manuscript. J.H. and T.Y. contributed substantially to revisions.

### Additional Information

**Supplementary information** accompanies this paper at <http://www.nature.com/srep>

**Competing financial interests:** The authors declare no competing financial interests.

**How to cite this article:** Zhou, L. *et al.* A novel self-enhanced electrochemiluminescence immunosensor based on hollow Ru-SiO<sub>2</sub>@PEI nanoparticles for NSE analysis. *Sci. Rep.* **6**, 22234; doi: 10.1038/srep22234 (2016).



This work is licensed under a Creative Commons Attribution 4.0 International License. The images or other third party material in this article are included in the article's Creative Commons license, unless indicated otherwise in the credit line; if the material is not included under the Creative Commons license, users will need to obtain permission from the license holder to reproduce the material. To view a copy of this license, visit <http://creativecommons.org/licenses/by/4.0/>